# Pickup proton instabilities and scattering in the distant solar wind and the outer heliosheath: Hybrid simulations

Kaijun Liu,[1,2] Eberhard Möbius,[1,3] S. Peter Gary,[1] and Dan Winske[1]

Received 18 May 2012; revised 30 July 2012; accepted 2 September 2012; published 6 October 2012.

[1] The growth of magnetic field fluctuations driven by the injection of pickup ions perpendicular to a background magnetic field in a homogeneous, collisionless plasma is studied using one-dimensional hybrid simulations. Freshly ionized protons are continuously injected into the simulations at constant rates and relative speeds consistent with conditions in the distant solar wind and the outer heliosheath. The pickup protons initially form a ring-velocity distribution unstable to the electromagnetic proton cyclotron instability and lead to enhanced magnetic fluctuations. After an exponential growth phase of the instability, the fluctuating magnetic fields exhibit linear temporal growth followed by a more-slowly growing quasi-steady phase. The excited fluctuations pitch angle scatter the pickup protons toward an isotropic shell velocity distribution with the most significant scattering occurring in the exponential growth phase. The scattering rate of the freshly injected pickup protons during the linear temporal growth phase remains relatively constant and it increases with the pickup proton injection rate. More importantly, significant pitch angle scattering only occurs after the accumulated pickup proton density exceeds a critical value, the scattering-onset density. The scattering-onset density also increases with the pickup proton injection rate and the scattering onset typically occurs during the exponential growth phase of the magnetic fluctuations. Scaling relations for the scattering rate and the scattering-onset density versus the pickup proton injection rate are derived from the simulation results. These relations suggest that significant scattering of pickup protons in the outer heliosheath occurs in a relatively limited spatial range close to the heliopause, related to the issue of whether the "secondary ENA" mechanism is a possible explanation for the ENA ribbon observed by IBEX. Implications of the results on pickup proton dynamics in the distant solar wind are also discussed.

**Citation:** Liu, K., E. Möbius, S. P. Gary, and D. Winske (2012), Pickup proton instabilities and scattering in the distant solar wind and the outer heliosheath: Hybrid simulations, *J. Geophys. Res.*, *117*, A10102, doi:10.1029/2012JA017969.

## 1. Introduction

[2] Pickup ions may arise whenever a magnetized plasma flows through a neutral gas. If a neutral atom is suddenly ionized, there are two limiting cases for the subsequent response of the newborn ion. If the plasma flow is strictly parallel to the background magnetic field, $\mathbf{B}_0$, the newborn ion will initially remain stationary, but if the plasma flow velocity is perpendicular to $\mathbf{B}_0$, the motional electric field will accelerate the newborn ion so that it has both a cyclotron motion and the average plasma flow velocity; that is, it is picked up by the flow.

[3] Figure 1 is a schematic illustration of plasma flows in the heliosphere and outer heliosheath. Our understanding of the global heliospheric dynamics has advanced greatly since the early pioneering work [e.g., *Axford et al.*, 1963; *Fahr*, 1968]. As interstellar neutrals, predominantly hydrogen atoms, flow into the heliosphere, they become ionized primarily through photoionization by solar EUV and charge exchange with solar wind plasma particles [*Bzowski et al.*, 2008]. These pickup ions are accumulated in the solar wind flow with increasing distance from the Sun, so that as the solar wind approaches the termination shock, pickup ions constitute about 20% of the plasma density [*Richardson*, 2008].

[4] The termination shock is the solar wind transition from super-magnetosonic to sub-magnetosonic flow. At this shock, there is appreciable heating of both the thermal solar wind ions and the suprathermal pickup ions, although it is the latter which gain the greater fraction of dissipated energy [*Richardson*, 2008; *Richardson et al.*, 2008a; *Wu et al.*, 2009; *Zank et al.*, 1996a]. Beyond the termination shock lies the inner heliosheath where the plasma flow is deflected in anticipation of the encounter with the heliopause, the boundary which separates the heliospheric plasma and magnetic fields from the plasma and fields of the local interstellar

[1]Los Alamos National Laboratory, Los Alamos, New Mexico, USA.
[2]Physics Department, Auburn University, Auburn, Alabama, USA.
[3]Space Science Center and Department of Physics, University of New Hampshire, Durham, New Hampshire, USA.

Corresponding author: K. Liu, Physics Department, Auburn University, Auburn, AL 36849, USA. (kaijun@auburn.edu)


0148-0227/12/2012JA017969

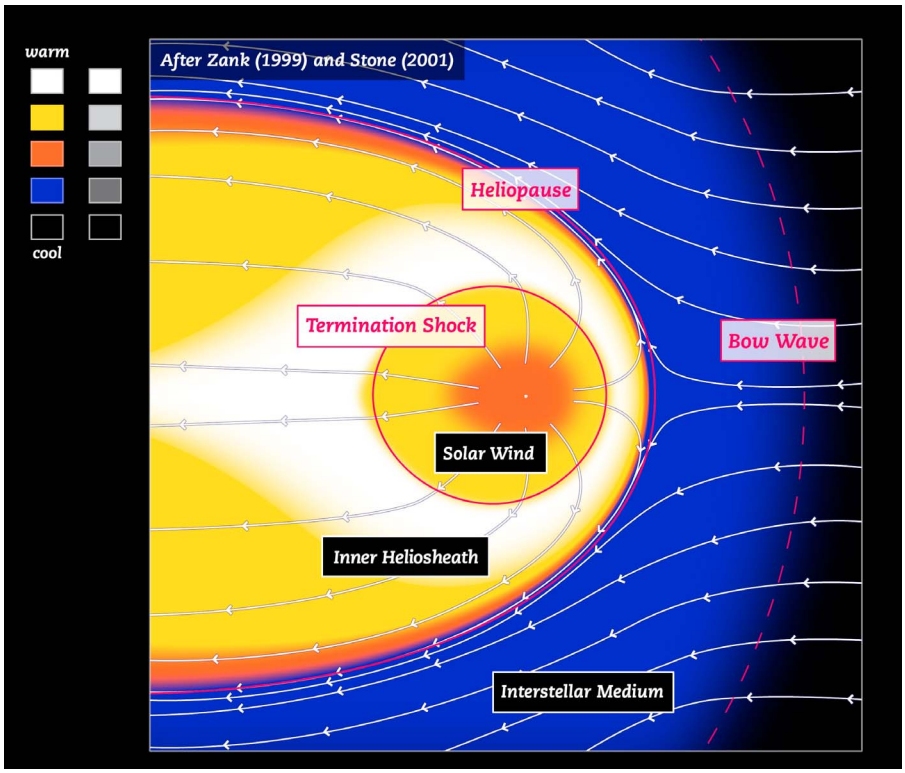


**Figure 1.** Schematic illustration of plasma flows in the heliosphere and outer heliosheath. Illustration by Giacomo Marchesi [after *Zank*, 1999; *Stone*, 2001].

medium. The region beyond the heliopause is termed the outer heliosheath, the transition zone where the interstellar plasma is slowed and diverted around the heliosphere. It was formerly widely expected that this region could contain a bow shock, a relatively sharp, super-magnetosonic-to-sub-magnetosonic transition in the flow of the interstellar medium, but whether such a shock exists has been disputed [*Zank et al.*, 1996b; *Richardson*, 1997]. Recent observations from the IBEX spacecraft [*McComas et al.*, 2012] demonstrate that this flow is sub-magnetosonic throughout the local interstellar medium and that the characterization of the flow transition is a bow wave, rather than a shock. Without the bow shock, the term "outer heliosheath" becomes inappropriate. However, in the present work, we bow to precedent and still refer to the relevant region as "outer heliosheath". Although solar wind plasma cannot flow directly into the outer heliosheath, the neutral particles from charge exchange on outward flowing solar wind ions can pass through the heliopause and permeate the outer heliosheath. There, these solar wind neutrals interact with neutrals and plasma from the interstellar medium via elastic collisions and charge exchange, respectively.

[5] Plasma instabilities play a fundamental role for pickup ion dynamics in the solar wind and heliosheath. We define the angle between the plasma flow and the background magnetic field as $\theta_{Bv}$. There are two extreme values of this angle which correspond to two very different regimes for ion pickup [*Omidi and Winske*, 1986]. If $\theta_{Bv} = 0°$, the accumulation of a sufficient density of injected ions leads to a magnetic field-aligned ion beam which will drive one of several possible ion/ion instabilities [*Gary*, 1991]. Linear theory for these growing modes is summarized by *Gary* [1993, chapter 8], and there are observations of such instabilities driven by newborn beams of both protons [*Murphy et al.*, 1995] and $He^+$ [*Joyce et al.*, 2010]. The instabilities pitch angle scatter the newborn beam, so that at sufficiently long times the injected ions attain zero average velocity in the plasma frame [*Gary et al.*, 1986]; that is, they become pickup ions.

[6] If the plasma flow is strictly perpendicular to $\mathbf{B}_0$, newborn ions will form a velocity-ring distribution in the frame of the plasma flow; that is, the injected ions become pickup ions within one cyclotron period. Velocity-ring distributions are unstable to two distinct categories of growing modes [*Joyce et al.*, 2012]. One category is that of electromagnetic cyclotron and Alfvén-cyclotron instabilities with frequencies $\omega \leq \Omega_p$, wave numbers $k\lambda_i \leq 1$ ($\lambda_i = c/\omega_p$ is the proton inertial length), and maximum growth rate at $\mathbf{k} \times \mathbf{B}_0 = 0$ [*Florinski et al.*, 2010, and references therein]. The other category consists of ion Bernstein mode instabilities with maximum growth rates at frequencies near harmonics of the ion cyclotron frequency, wave numbers $k_\perp v_j/\Omega_j \geq 1$, where $j$ denotes the ion species, and wave vectors almost perpendicular to $\mathbf{B}_0$ [*Liu et al.*, 2011]. (See Appendix A for definitions of the symbols used here.)

[7] With the exception of very low $\beta$ plasmas, both types of free energy, as well as the more general case of ring beam pickup ion velocity distributions, are more likely to excite electromagnetic instabilities than electrostatic growing modes. For the case of interest here, in which the pickup ion initial speed is much greater than the Alfvén speed, enhanced fluctuations from electromagnetic ion/ion instabilities or the velocity-ring cyclotron instability pitch angle scatter the

pickup ion distribution into a thin, relatively isotropic velocity shell. This has been illustrated by hybrid simulations for pickup ions in solar wind/cometary environments [*Wu et al.*, 1986; *Gary et al.*, 1986, 1988, 1989, 1991] as well as in the outer heliosheath [*Florinski et al.*, 2010]. If the simulations are extended to much longer times, the pickup ions will be scattered in energy, thereby broadening the spherical velocity shell distribution. On still longer times associated with Coulomb collisions, the pickup ion velocity distributions evolve to a Maxwellian-like condition. But as long as the instability frequency $\omega$ satisfies $\omega \leq \Omega_p$, magnetic fluctuations will dominate electric field fluctuations and pitch angle scattering will be the fastest pickup ion transport process. In addition, in the expanding solar wind, the evolution of the pickup ion velocity distributions is further complicated by the adiabatic cooling associated with the decrease of the interplanetary magnetic field strength as the solar wind flows away from the Sun [*Vasyliunas and Siscoe*, 1976].

[8] Our goal here is to use hybrid simulations to quantify the dynamics of pickup protons and the associated proton cyclotron instability for conditions appropriate to the distant solar wind and the outer heliosheath. We consider a homogeneous electron-proton plasma with a uniform background magnetic field $\mathbf{B}_0$. Pickup protons are added to the plasma uniformly in space at a dimensionless rate

$$\nu_{pu} \equiv \left(\frac{dn_{pu}}{dt}\right)\frac{1}{n_0\Omega_p}, \tag{1}$$

where $n_0$ is the density of the background plasma. This gradual addition of nonthermal ions represents a temporal increase in the plasma free energy, leading to the growth of plasma instabilities, the development of enhanced field fluctuations, and the scattering of the pickup protons. For simplicity, the present simulations use constant $\nu_{pu}$ and the pickup protons are injected with velocities perpendicular to $\mathbf{B}_0$. Our simulations use a one-dimensional simulation box along $\mathbf{B}_0$, so it is the electromagnetic proton cyclotron instabilities at $\mathbf{k} \times \mathbf{B}_0 = 0$ [*Gary and Madland*, 1988] which are the normal modes of the growing fluctuations. Notice that our use of a temporally increasing pickup proton density follows the cometary pickup ion simulations of *Gary et al.* [1986, 1988, 1989, 1991], but is fundamentally different from the simulations of *Wu et al.* [1986] and *Florinski et al.* [2010] who assume an initial pickup ion velocity distribution of constant density and then compute the subsequent plasma response.

[9] If the pickup proton injection rate is constant and sufficiently weak, hybrid simulations show that, at sufficiently late times, the magnetic field fluctuations exhibit an interval of linear temporal growth [*Gary et al.*, 1986], so that we may write

$$\frac{d}{dt}\left(\frac{\delta B^2}{8\pi}\right) = \sigma_{pu}\frac{dn_{pu}}{dt}\frac{m_p v_{pu}^2}{2}, \tag{2}$$

where $v_{pu}$ is the injection speed of the pickup protons and $\sigma_{pu}$ is a dimensionless factor independent of time. Note that $\sigma_{pu}$ represents the ratio of the magnetic field energy density growth rate to the injection rate of the pickup proton energy density, so it is essentially an efficiency factor measuring the energy conversion from the kinetic energy of the injected pickup protons to the energy of the magnetic field fluctuations.

[10] Using equation (1), one can rewrite equation (2) into a dimensionless form

$$\frac{d}{\Omega_p dt}\left(\frac{\delta B^2}{B_0^2}\right) = \sigma_{pu}\nu_{pu}\frac{v_{pu}^2}{v_A^2}. \tag{3}$$

Our previous work has shown that linear temporal growth of the magnetic fluctuations driven by pickup ion injection becomes a more appropriate response as $\theta_{Bv}$ approaches 90° [see *Gary et al.*, 1989, Figure 3] and when the pickup ions are protons rather than heavy ions [see *Gary et al.*, 1988, Figure 1]. Both of these conditions are satisfied in the simulations described here.

[11] The paper is organized as follows. Section 2 introduces the energetic neutral atom (ENA) ribbon observed by IBEX and one leading ribbon scenario related to pickup ions in the outer heliosheath. Section 3 describes an analytic model for average pickup ion injection rates and injection speeds in the solar wind as well as other relevant solar wind parameters, which provides parameter values for use in the subsequent simulations described in section 4. Section 4 also discusses the implications of the present simulation results on the pickup proton dynamics in the distant solar wind and the outer heliosheath. Finally, section 5 summarizes the conclusions and points out several limitations of the study.

## 2. IBEX Observations: Scenarios for the "Ribbon"

[12] The Interstellar Boundary Explorer (IBEX) [*McComas et al.*, 2004] is an Earth-orbiting satellite launched in October 2008 with the single objective of discovering the global interaction between the solar wind and the interstellar medium. IBEX carries two highly sensitive ENA imaging sensors that measure neutral atoms from 10 eV to 6 keV. In look directions away from the vicinity of Earth, two important sources of such neutrals should be the inner heliosheath and the outer heliosheath. Thus, the IBEX measurements provide new information about how the heliosphere interacts with the local interstellar cloud through which we are moving [*McComas et al.*, 2009, 2010; *Fuselier et al.*, 2009; *Schwadron et al.*, 2009].

[13] The most dramatic discovery from IBEX has been the observation of a three-fold enhancement of ENAs near 1 keV in a nearly circular ribbon in the sky [*McComas et al.*, 2009, 2010] but not along a "great circle" [*Funsten et al.*, 2009]. This ribbon was not predicted by any pre-IBEX theories or models and remains the source of intense speculation and modeling [*Schwadron et al.*, 2009; *Heerikhuisen et al.*, 2010]. *McComas et al.* [2009, 2010] summarize six different plasma mechanisms which may produce enhanced fluxes of ENAs and therefore may be possible sources of the IBEX ribbon. One of the leading mechanisms, the "secondary ENA" mechanism, starts with the thermal solar wind plasma flowing anti-sunward at approximately 400 km/s. These ions undergo charge exchange with interstellar neutrals in the heliosphere and become ENAs; as neutrals they continue their outward flow across the heliopause into the outer heliosheath. There they undergo a second charge exchange with cold interstellar ions, becoming energetic

(~1 keV) pickup ions with a ring beam velocity distribution with orientation determined by the interstellar magnetic field. These pickup ions can undergo a third charge exchange, again with interstellar neutrals, but on a rather slow timescale. In this way, a Sunward-directed flux of secondary ENAs is generated, which eventually may be detected by IBEX. A major difficulty for this mechanism is that, to achieve the observed ENA flux levels in the ribbon, a long line-of-sight integration on the order of one hundred AU or more appears to be required, so that the narrow velocity-ring distribution of these secondary pickup ions must be maintained for many years. However, the probability of Coulomb scattering and in particular scattering by pickup ion instabilities [*Florinski et al.*, 2010] may become large enough to broaden the ion pitch angle distributions and thereby destroy the coherence which leads to observations of a narrow ribbon. On the other hand, in contrast to the simulation results of *Florinski et al.* [2010], the analytic study of *Gamayunov et al.* [2010] suggests that a prescribed combination of the large-scale interstellar turbulence and a small-scale turbulence generated by the unstable narrow velocity-ring distribution of the pickup ions only broadens the pickup ion distribution slightly before the instability growth becomes quenched, so the narrow velocity-ring distribution of the secondary pickup ions can be maintained.

## 3. Model for Pickup Ion Injection Rates in the Solar Wind

[14] An analytic model for average pickup ion injection rates and injection speeds in the solar wind as well as other relevant solar wind parameters is developed to provide parameter values for use in the simulations described in section 4. For the solar wind at 1 AU, we have taken $n_{sw}$ = 5 cm$^{-3}$ and a flow speed of 440 km/s. Since the main purpose of the analytic model is to provide general guidance on input parameters to the subsequent hybrid simulations, the solar wind velocity is assumed to be a constant out to the termination shock for simplicity and the slowdown of the solar wind is not considered in the model [*Richardson et al.*, 2008b]. We have treated the interplanetary magnetic field as an ideal Parker spiral with $B_0$ = 5 nT at 1 AU. To calculate the $\beta$ of the cool solar wind protons, we used a temperature $T_{sw} = 10^5/R + 200R$ with $R$ (distance from the Sun) in AU to approximately match Voyager observations as given by *Isenberg et al.* [2010].

[15] Equation (2) suggests that the pickup ion injection rate $dn_{pu}/dt$ is a major determining factor of the growth rate of enhanced magnetic fluctuations from pickup-ion-driven instabilities, and for the subsequent scattering of the pickup ion velocity distributions. This rate can be written as

$$\frac{dn_{pu}}{dt} = \nu_{ion} n_j, \tag{4}$$

where $\nu_{ion}$ is the ionization rate per neutral atom and $n_j$ is the density of the $j$th neutral species. The ionization rate consists of photo-ionization due to solar EUV, charge exchange with the solar wind, and electron impact ionization, the first two of which scale as $1/R^2$ with distance from the Sun, while the latter typically falls off faster with distance because the electron distribution is cooling in the expanding solar wind. The ionization rates for H are described in detail in *Bzowski et al.* [2008] and for He in *Bzowski et al.* [2012]. The density $n_j$ of interstellar neutrals is almost constant throughout the heliosphere, except for the characteristic ionization cavity close to the Sun (within a few AU) where the density falls off roughly exponentially with inverse distance from the Sun [*Axford*, 1972]. The combination of the behaviors of the ionization rate and the neutral density leads to a variation of the pickup ion injection rate with a distinct maximum at a fraction of an AU for $He^+$ and at a few AU for $H^+$, varying with the total ionization rate in concert with solar activity.

[16] We have computed the variation of the dimensionless injection rates for protons and $He^+$ defined by equation (1) as a function of $R$ in the upwind direction of the interstellar flow. The $1/R^2$ dependences of the ionization rate and the solar wind density cancel in the dimensionless form, and only the $1/R$ dependence of the dominating azimuthal component of the interplanetary magnetic field survives as the most important factor in $\nu_{pu}$. To capture the average behavior, we have adopted interstellar gas parameters at the termination shock according to *Bzowski et al.* [2008] for H ($n_H$ = 0.08 cm$^{-3}$) as well as *Bzowski et al.* [2012] and *Möbius et al.* [2012] for He ($n_{He}$ = 0.015 cm$^{-3}$, $v_{He\infty}$ = 23.2 km/s). As average ionization rates at 1 AU we have used 6.1 × 10$^{-7}$ s$^{-1}$ for H [*Bzowski et al.*, 2008] and 1 × 10$^{-7}$ s$^{-1}$ for He [*Bzowski et al.*, 2012] as values for moderate solar activity.

[17] Results from this model as functions of $R$ are shown in Figure 2. Figure 2a shows the dimensionless solar wind speed $v_{sw}/v_A$ and Figure 2b illustrates $\beta_{sw}$. The dimensionless solar wind speed, which is approximately the pickup ion injection velocity, monotonically increases to an asymptotic value of $v_{sw}/v_A \simeq 13.5$ at $R \geq 10$ AU. Figure 2c illustrates $\nu_{pu}$ for both pickup protons and pickup $He^+$. At large distances from the Sun, both dimensionless injection rates increase linearly with $R$: over $10 \leq R \leq 100$, the proton rate can be fit by $\nu_{pu} = 3.0 \times 10^{-8} R - 1.0 \times 10^{-7}$, and the $He^+$ rate is well fit by $\nu_{pu} = 9.0 \times 10^{-10} R$. Figure 2d illustrates the ratio of pickup proton density to the cool proton solar wind density. The prediction that $n_{pu}/n_{sw} \simeq 0.3$ near the termination shock at $R \simeq 100$ AU testifies to the qualitative validity of the model.

## 4. Simulations

[18] One-dimensional, self-consistent hybrid simulations are carried out to study the dynamics of pickup protons in the distant solar wind ($R > 10$ AU) and the outer heliosheath. In the Los Alamos hybrid code used here, plasma ions are represented as superparticles, while electrons are treated as a massless, charge-neutralizing, adiabatic fluid with $\gamma$ = 5/3 [*Winske and Omidi*, 1993]. This is a robust, well-documented simulation code that has been extensively used to study various electromagnetic ion-driven instabilities in a broad range of space plasma physics applications [*Winske and Leroy*, 1984; *Gary et al.*, 1986; *Winske and Quest*, 1988; *McKean et al.*, 1995].

[19] Our simulations use a one-dimensional periodic simulation box along $\mathbf{B}_0$ and have all been run with the following configuration: The background (solar wind or interstellar) protons are constant in number density $n_0$ and initially are distributed uniformly in space with a Maxwellian velocity

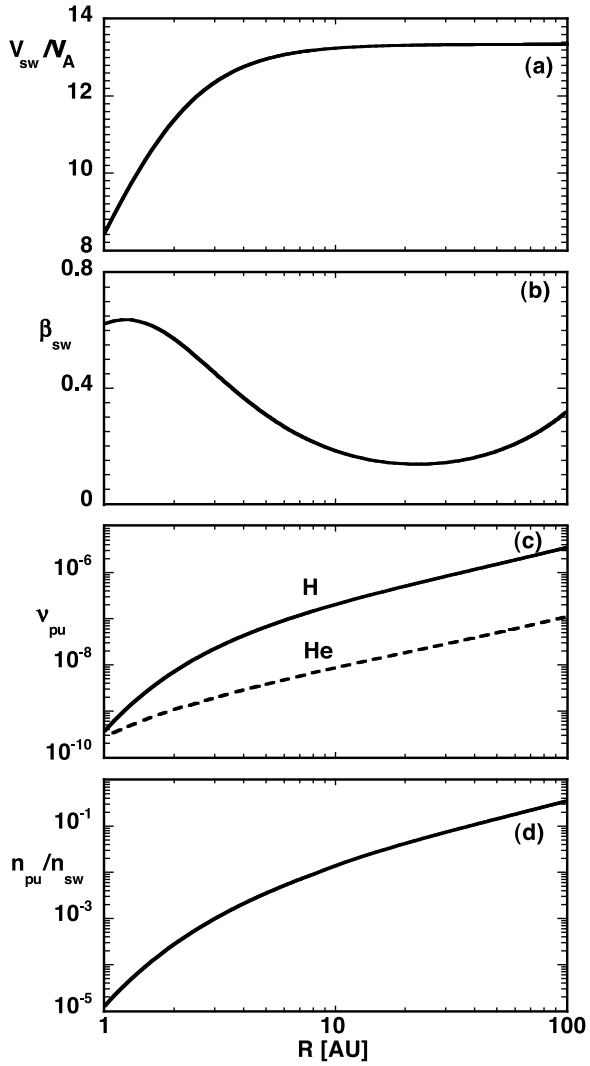


**Figure 2.** Results from the analytic model for pickup ion injection rates and injection speeds in the solar wind as well as other relevant solar wind parameters as described in Section 3. All quantities are functions of the distance from the Sun ($R$) along the upwind direction of the interstellar flow. (a) The solar wind speed, (b) the $\beta$ of the cool proton component of the solar wind, (c) the dimensionless pickup ion injection rate $\nu_{pu}$ for protons (solid line) and $He^+$ (dashed line), and (d) the ratio of pickup proton density to the cool proton solar wind density.

distribution. The simulations are carried out in the frame of this proton component. The pickup protons are introduced into the simulation randomly in space at a constant dimensionless rate with initial velocity $\mathbf{v}_{pu}$ perpendicular to $\mathbf{B}_0$. The simulations basically mimic plasmas with a gradual accumulation of pickup protons. With simplifications, this represents a plasma parcel moving toward the termination shock in the distant solar wind, while in the outer heliosheath, it simulates a plasma parcel approaching the heliopause from a far distance in the direction of the ENA ribbon observed by IBEX.

[20] Unless stated otherwise, other simulation parameters are $\beta_0 = 0.2$, $c/v_A = 10^4$, and $T_e/T_0 = 1$. The one-dimensional character of the simulations allows growth only of the electromagnetic proton cyclotron and Alfvén-cyclotron modes at $\mathbf{k} \times \mathbf{B}_0 = 0$. The simulation box size is 512 $\lambda_i$, the number of cells is 1024, the computational time step is $\Delta t\Omega_p = 0.02$, and each simulation uses 10000 superparticles per cell to represent the background protons. For convenience, the pickup protons are not injected into the system at every time step, but instead are injected 2000 times evenly spread across the course of each simulation. At each injection, 5120 superparticles (with a weight according to the injection rate and typically much smaller than the weight of the superparticles representing the background protons) are introduced with a ring-velocity distribution to represent pickup protons. This makes the results statistically significant as we later investigate the scattering of the pickup protons injected at each time. In addition, this leads to 10000 superparticles per cell representing the pickup protons at the end of each simulation, same as the number of the superparticles representing the background protons. Finally, it is worth noting that the time interval between two consecutive injections is very short compared with the timescales of the instability development and the pickup proton scattering. Thus, the injection is still effectively continuous. Test simulations with shorter injection intervals have been performed and the results remain essentially the same.

### 4.1. A Representative Simulation

[21] We first carried out a representative simulation with $\nu_{pu} = 1.0 \times 10^{-6}$ and $v_{pu}/v_A = 10.0$ (corresponding to $v_{pu} = 300$ km/s). Figure 3a shows the evolution of the total fluctuating magnetic field energy density. At early times there are insufficient pickup protons to drive wave growth and the system is in a relatively quiescent phase, but at $2000 \leq t\Omega_p \leq 2400$ the electromagnetic proton cyclotron instability arises with exponential temporal growth. After that, the magnetic fluctuations enter a phase of approximately linear temporal growth over $2800 \leq t\Omega_p \leq 10000$; in this regime equation (3) is satisfied with $\sigma_{pu} \simeq 0.0071$. At still later times, the fluctuating fields tend toward a quasi-steady state of even slower growth. A similar temporal response of the magnetic fluctuation energy is shown in *Cowee et al.* [2008, Figure 1a] which illustrates a hybrid

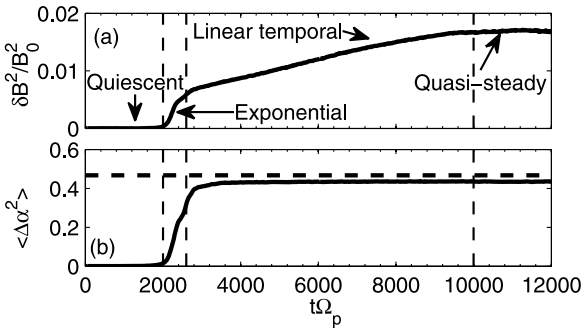


**Figure 3.** Results as functions of time from the representative simulation with $\nu_{pu} = 1.0 \times 10^{-6}$ and $v_{pu}/v_A = 10.0$. (a) Total fluctuating magnetic field energy density, (b) the mean square pitch angle change of the pickup protons. The vertical dashed lines in both Figures 3a and 3b approximately separate the four different phases of the wave growth. The horizontal dashed line in Figure 3b marks $\langle \Delta\alpha^2 \rangle = 0.467$.

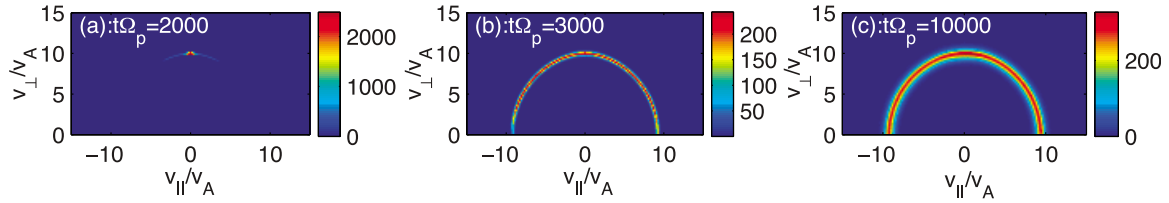


**Figure 4.** The pickup proton velocity distributions in the $v_\perp - v_\parallel$ phase space from the representative simulation at three simulation times as labeled.

simulation of perpendicular injection of pickup ions at sub-Alfvénic velocities.

[22] Associated with the growth of the magnetic fluctuations, pickup protons injected into the system are scattered in pitch angle due to wave-particle interactions. The evolution of $\langle \Delta\alpha^2 \rangle$, the mean square pitch angle change of the pickup protons in this representative simulation, is displayed in Figure 3b. Here $\Delta\alpha = \alpha - \alpha_0$ and $\alpha_0 = \pi/2$ is the value of the initial pitch angles of the pickup protons. Before the exponential growth phase of the wave energy, there is no appreciable scattering of the pickup protons. When the fluctuating fields enter their exponential growth phase, $\langle \Delta\alpha^2 \rangle$ also grows very rapidly. After that, $\langle \Delta\alpha^2 \rangle$ starts to slowly approach an asymptotic value of $(\pi^2 - 8)/4 = 0.467$, which corresponds to an isotropic distribution in pitch angle. During the course of the simulation, the pickup proton density increases linearly with time as they are injected at a constant rate. We define the pickup proton density when $\langle \Delta\alpha^2 \rangle$ of the pickup protons exceeds 0.2 (corresponding to $\sqrt{\langle \Delta\alpha^2 \rangle} = 25.6^\circ$) as the scattering-onset density, $n_{onset}$, which is a measure of how many pickup ions are needed, for a given injection rate, to drive the waves to a sufficient level so that the pickup protons are significantly pitch angle scattered. In the representative simulation, $n_{onset}/n_0 = 2.4 \times 10^{-3}$. As shown by the representative simulation of Figure 3 and other simulations discussed in section 4.2, the scattering onset typically occurs during the exponential growth phase of the magnetic fluctuations.

[23] To more clearly demonstrate the scattering of the pickup protons, Figure 4 illustrates the pickup proton velocity distributions at three times during the representative simulation. The pickup proton velocity distribution right before the exponential wave growth phase is shown in Figure 4a, which clearly demonstrates a ring distribution, consistent with Figure 3 that the waves are still sufficiently weak and the pickup ions have not been significantly scattered at this moment. Figure 4b displays the pickup proton velocity distribution at $t\Omega_p = 3000$, near the beginning of the linear temporal growth phase of the wave energy. The pickup protons have now been substantially scattered in pitch angle, consistent with a quasi-linear model in which pitch angle broadening of the pickup proton distribution leads to a substantial decrease in the instability growth rate [*Gary and Madland*, 1988]. During the linear temporal growth phase, the pickup proton velocity distribution continues to broaden toward a fully isotropic velocity shell, as shown by Figure 4c.

[24] Figure 5 presents the fluctuating magnetic field energy spectral densities as functions of wave number at four simulation times. In addition to the monotonic increase in the total magnetic fluctuation energy density with time as indicated in Figure 3a, the spectra show that the wave growth during the linear temporal growth phase mainly comes from the long wavelength range of $k\lambda_i < 0.1$, while the wave spectra at $k\lambda_i > 0.1$ remain relatively the same. A similar trend has been demonstrated by *Cowee et al.* [2008, Figure 3]. This is also consistent with the linear theory prediction that the maximum growth rate should move to smaller values of $k$ as the pickup protons become more strongly scattered [*Gary and Madland*, 1988]. The proton cyclotron resonance condition, $\omega - k_\parallel v_\parallel = \Omega_p$, implies that the freshly injected pickup protons at relatively small $v_\parallel$ should be most strongly scattered by the large $k_\parallel$ short-wavelength fluctuations, whereas the protons scattered to small pitch angles should further interact primarily with much longer wavelength modes.

[25] Figure 3b demonstrates the squared pitch angle change averaged over all the pickup protons, therefore, it does not clearly reveal the scattering rate of the freshly injected pickup protons at different simulation times as the number of the newly injected protons becomes very small compared to the number of the previously injected protons. In order to investigate the scattering rate of the freshly injected pickup protons at different simulation times, we calculate the mean square pitch angle change of the pickup protons injected at specified simulation times and the results are shown in Figure 6. The black curve in Figure 6 shows that the scattering of the freshly injected pickup protons is relatively slow during early phase of the exponential growth of the wave energy, while the other three curves demonstrate that the freshly injected pickup protons are scattered at comparable rates during the linear temporal growth phase of the wave energy. This is indeed consistent with the relatively unchanged wave energy spectral densities at $k\lambda_i > 0.1$ during

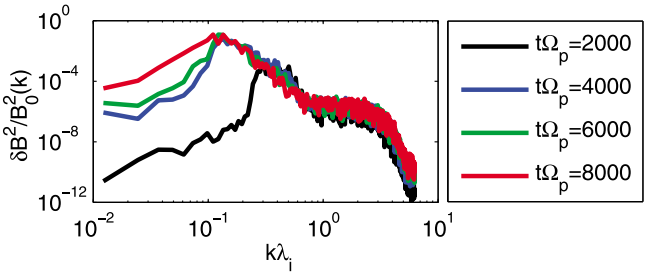


**Figure 5.** The fluctuating magnetic field energy spectral densities as functions of wave number from the representative simulation at four simulation times as labeled. Each spectrum is obtained by averaging the spectrum over 100 simulation time steps around the respective simulation time to reduce noise.

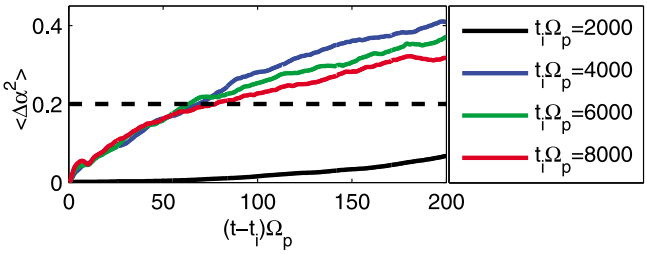


**Figure 6.** The mean square pitch angle change of the pickup protons injected at four specified simulation times from the representative simulation. The x-axis represents the time from the corresponding injection time ($t_i$) for each individual curve as labeled. The horizontal dashed-line marks $\langle \Delta\alpha^2 \rangle = 0.2$.

the linear temporal growth phase, as shown in Figure 5. If one assumes that the enhanced waves in the simulation approximately follow the cold plasma dispersion relation for electromagnetic ion cyclotron waves in an electron-proton plasma, $k\lambda_i = (\omega/\Omega_p)/\sqrt{1-\omega/\Omega_p}$, using the proton cyclotron resonance condition of $\omega - k_{\|}v_{\|} = \Omega_p$ and the parameters of the representative simulation, one finds that the protons with $30^\circ < \alpha < 150^\circ$ resonate with waves of $k\lambda_i > 0.1$ only. So the waves of $k\lambda_i > 0.1$ are the effective waves in scattering the newly injected pickup protons. Although the total fluctuating magnetic field energy continues to increase throughout the linear temporal growth phase, the field energy available to effectively scatter the freshly injected pickup protons remains relatively constant. This makes it plausible to characterize the pitch angle scattering of those particles in the linear temporal growth phase via a constant scattering time, $t_s$, as described below.

[26] In the present work, we define $t_s$ as the time it takes for $\langle \Delta\alpha^2 \rangle$ of the newly injected pickup protons to exceed 0.2. It is an approximate measure of how fast these protons are significantly scattered. We calculate $t_s$ near the beginning, in the middle, and near the end of the linear temporal growth phase in each simulation and use their mean as the final scattering time. In Figure 6, the three scattering times measured are $t_s\Omega_p = 69$, 64, and 78 at $t\Omega_p = 4000$, 6000, and 8000, respectively, which gives an average scattering time of $t_s\Omega_p = 70$ ($\sim$11 proton cyclotron periods).

### 4.2. Ensembles of Simulations

[27] We first perform four ensembles of simulations to investigate how $\sigma_{pu}$ varies with $\nu_{pu}$ and other plasma parameters. The four simulation ensembles are set up as follows: Ensemble One corresponds to $v_{pu}/v_A = 10.0$, $\beta_0 = 0.2$, but several different values of the pickup proton injection rate. Ensemble Two corresponds to $v_{pu}/v_A = 10.0$, $\beta_0 = 1.0$, but several different values of the pickup proton injection rate. Ensemble Three corresponds to $\nu_{pu} = 1.0 \times 10^{-6}$, $\beta_0 = 0.2$, but several different values of the pickup proton injection speed. Ensemble Four corresponds to $\nu_{pu} = 1.0 \times 10^{-6}$, $\beta_0 = 1.0$, but several different values of the pickup proton injection speed.

[28] Figure 7a shows $\sigma_{pu}$ as functions of $\nu_{pu}$ obtained from the linear temporal growth intervals of Ensembles One and Two. Figure 7b displays $\sigma_{pu}$ as functions of $v_{pu}/v_A$ obtained from the linear temporal growth intervals of Ensembles Three and Four. The most important result here is that $\sigma_{pu}$ is essentially independent of both the pickup proton injection rate and the pickup proton injection speed; the only consistent variation is that the larger $\beta_0$ corresponds to the smaller values of $\sigma_{pu}$. Our interpretation here is that this is simply due to the stronger proton cyclotron damping associated with larger values of $\beta_0$. The interpretation is consistent with the simulation results that the background protons experience transverse heating associated with the wave growth and the absolute amount of heating is larger in simulations with larger values of $\beta_0$.

[29] The "secondary ENA" mechanism for the narrow ENA ribbon observed by IBEX requires that the pickup protons in the outer heliosheath maintain their narrow velocity-ring distribution for a long time. Here we carry out an ensemble of simulations with different $\nu_{pu}$ to investigate how $t_s$ and $n_{onset}$ change with $\nu_{pu}$ under conditions typical to the outer heliosheath. For this ensemble of simulations, we use $\beta_0 = 0.2$ and $c/v_A = 1.5 \times 10^4$ to represent the interstellar protons in the outer heliosheath ($n_0 = 0.1$ cm$^{-3}$, $B_0 = 0.30$ nT, and $T_0 = 6400$ K). The pickup proton injection velocity is chosen to be $v_{pu}/v_A = 20.0$ (corresponding to $v_{pu} = 400$ km/s) and perpendicular to $\mathbf{B}_0$. All other parameters remain unchanged. The pickup proton injection rate in the outer heliosheath is much smaller than the one in the distant solar wind due to the very small solar wind neutral density in this region. It is difficult to run simulations at pickup proton injection rates typical for the outer heliosheath, because such small values require very large numbers of simulation particles per cell to reduce thermal noise and consequently exceptionally long run times. We here, instead, use relatively

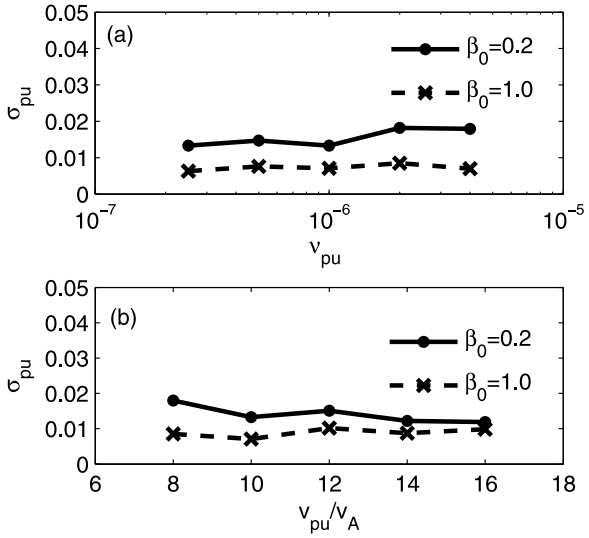


**Figure 7.** The energy conversion factor $\sigma_{pu}$ defined in equation (3), calculated over the linear temporal growth phase of the fluctuating magnetic field energy. (a) $\sigma_{pu}$ as a function of the pickup proton injection rate from Ensemble One ($\beta_0 = 0.2$; the solid line) and from Ensemble Two ($\beta_0 = 1.0$; the dashed line). (b) $\sigma_{pu}$ as a function of the pickup proton injection speed from Ensemble Three ($\beta_0 = 0.2$; the solid line) and from Ensemble Four ($\beta_0 = 1.0$; the dashed line).

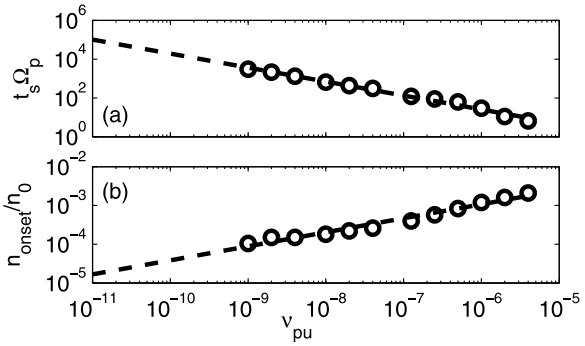


**Figure 8.** The scattering time $t_s$ and the scattering onset density $n_{onset}$ as defined in section 4.1 calculated from an ensemble of simulations with $\beta_0 = 0.2$, $c/v_A = 1.5 \times 10^4$, and $v_{pu}/v_A = 20.0$. (a) $t_s$ as a function of the pickup proton injection rate. (b) $n_{onset}$ as a function of the pickup proton injection rate.

large $\nu_{pu}$ but vary it over several orders of magnitude and then extrapolate the results to appropriate values of the injection rate in the outer heliosheath.

[30] Figures 8a and 8b present the simulated $t_s$ and $n_{onset}$ as functions of $\nu_{pu}$, respectively. The dashed lines represent numerical fits of $t_s$ and $n_{onset}$: $t_s\Omega_p = 0.0012\nu_{pu}^{-0.72}$ and $n_{onset}/n_0 = 0.16\nu_{pu}^{0.36}$. Clearly, $t_s$ decreases with increasing $\nu_{pu}$. This implies an increasing scattering rate ($\sim 1/t_s$) when the pickup proton injection rate increases. More interestingly, $n_{onset}$ increases with increasing $\nu_{pu}$. This seems to be counter-intuitive but can be understood as follows. As the pickup protons accumulate in the simulations with time, instabilities gradually start to develop which requires some form of coherent coupling between the fluctuations and the pickup protons already injected. At the same time, the newly injected pickup protons have not had time to couple themselves accordingly to the waves, so they tend to weaken the development of coherent coupling. Therefore, a larger injection rate leads to a stronger damping effect on wave growth and delays the wave growth (and the subsequent pickup proton scattering) until more pickup protons have been accumulated for wave growth to overcome this effect.

### 4.3. Implications for the Outer Heliosheath

[31] The typical pickup proton injection rate in the outer heliosheath near the heliopause is $\nu_{pu} = 5 \times 10^{-11}$, which has been estimated using an approximate solar wind neutral density of $2 \times 10^{-5}$ cm$^{-3}$, a charge exchange cross section of $1.70 \times 10^{-15}$ cm$^2$ [*Lindsay and Stebbings*, 2005], a solar wind neutral velocity of 400 km/s, and $B_0 = 0.30$ nT. It is difficult to carry out hybrid simulations for such a small injection rate. If we assume the scaling relations derived above remain valid for such a small injection rate, we get $t_s\Omega_p = 3.1 \times 10^4$ and $n_{onset}/n_0 = 3.1 \times 10^{-5}$. Using $B_0 = 0.30$ nT in the outer heliosheath, one finds $\Omega_p = 0.029$ Hz and $t_s = 12$ days. This is considerably shorter than the minimum scattering timescale of years required to maintain the validity of the "secondary ENA" mechanism [*Heerikhuisen et al.*, 2010]. Note that, in *Florinski et al.* [2010], the pickup ions are assumed to be present initially in the simulations with a constant density of $n_{pu}/n_0 = 1.8 \times 10^{-4}$ in the outer heliosheath. Their results suggested a scattering time on the order of days, which is even shorter than our estimate of 12 days. This difference is due to the fact that the present simulations gradually inject pickup protons and therefore the free energy is gradually increased rather than all introduced initially. In addition, although the estimated scattering time of $t_s = 12$ days here implies a rapid scattering that could invalidate the "secondary ENA" mechanism, this scattering time is for the linear temporal growth phase of the instability which occurs only after the pickup proton density has exceeded $n_{onset}$. Thus, as will be discussed in the next paragraph, the "secondary ENA" mechanism can still be effective far outside of the heliopause where the pickup proton density is small.

[32] As the interstellar plasma in the outer heliosheath approaches the heliopause, pickup protons slowly accumulate. The value of $n_{onset}$ reveals when the waves excited by these pickup protons grow to a significant level so that the pickup protons are substantially scattered. The estimate of $n_{onset}/n_0 = 3.1 \times 10^{-5}$, which is 17% of $n_{pu}/n_0 = 1.8 \times 10^{-4}$ used in the work of *Florinski et al.* [2010], suggests that sufficiently far outside of the heliopause, the plasma can still be in the quiescent phase of the wave growth and all the pickup protons remain as a narrow velocity ring. When the plasma arrives at a critical distance from the heliopause, the accumulated pickup proton density exceeds the scattering-onset density (determined by the local injection rate), the waves driven by the pickup protons start to grow exponentially and the pickup protons are subsequently scattered in pitch angle. After that, the plasma enters the linear temporal growth phase and the scattering time of the newly injected pickup protons is determined by $t_s$. Therefore, although the estimated scattering time near the heliopause, $t_s = 12$ days, is short enough to broaden the pickup ion velocity distribution on the order of 10 days, it is possible that the scattering onset of the pickup protons does not occur until relatively close to the heliopause, so that the pickup protons outside of this scattering-onset distance remain as a narrow velocity ring and may lead to the narrow ENA ribbon observed by IBEX.

[33] According to *Florinski et al.* [2010], the observed ENA ribbon intensity requires $n_{pu}/n_0 = 1.8 \times 10^{-4}$ if the line of sight integral length is 200 AU. However, their derivation assumes that the pickup ions are uniformly distributed over $2\pi$ of solid angle in velocity space (see equation (2) and the related discussion of *Florinski et al.* [2010]). This corresponds to a partial shell velocity distribution within a pitch angle range of $60° < \alpha < 120°$ (see equation (12) and the related discussion of *Florinski et al.* [2010]). So, our estimate of $n_{onset}/n_0 = 3.1 \times 10^{-5}$, which is 17% of $n_{pu}/n_0 = 1.8 \times 10^{-4}$ used in the work of *Florinski et al.* [2010], is still capable of reproducing the observed ENA ribbon intensity as long as the pickup ion distribution remains narrow enough, i.e., $85° < \alpha < 95°$. On the other hand, the pickup ion density in the outer heliosheath decreases with distance from the heliopause and is certainly not a constant across 200 AU as assumed in *Florinski et al.* [2010]. A further investigation of the present scenario in a global model is presently underway to give a more accurate estimate of the ENA ribbon intensity.

### 4.4. Implications for the Distant Solar Wind

[34] In the distant solar wind, our results suggest that the plasma has passed the scattering-onset point given the quick

accumulation of the pickup protons. The linear temporal growth phase of the wave energy is then relevant. The scattering time given by Figure 6 for the representative run is $t_s\Omega_p = 70$. If we concentrate on the upstream of the termination shock at $R \simeq 100$ AU, $B_0 \approx 0.03$ nT and $\Omega_p \approx 0.003$ Hz. So $t_s \simeq 6$ hours, which is significantly shorter than the solar wind transport time as the solar wind travels only 0.06 AU in 6 hours, assuming $v_{sw} = 400$ km/s.

[35] Since $\sigma_{pu}$ is essentially independent of both the pickup proton injection rate and the pickup proton injection speed, one can integrate equation (3) over time to estimate the total wave energy excited by the pickup protons,

$$\frac{\delta B^2}{B_0^2} = \sigma_{pu}\frac{n_{pu}}{n_0}\frac{v_{pu}^2}{v_A^2}, \tag{5}$$

where $v_{pu}/v_A$ has been assumed to be a constant and the energy conversion factors from the kinetic energy of the injected pickup protons to the energy of the magnetic fluctuations during the quiescent phase, the exponential growth phase, and the late-time quasi-steady phase of the instability have all been approximated with $\sigma_{pu}$ in the linear temporal growth phase.

[36] Equation (5) suggests that the total wave energy driven by the pickup protons is approximately a fraction of the total pickup proton kinetic energy at a given location in the distant solar wind. For example, Figure 2d shows that the pickup proton density is $n_{pu}/n_{sw} \simeq 0.3$ upstream of the termination shock at $R \simeq 100$ AU. If we assume that $v_{pu}/v_A = 10$ and use $\sigma_{pu} \simeq 0.01$ as suggested by Figure 7, we get $(\delta B/B_0)^2 \simeq n_{pu}/n_{sw} \simeq 0.3$. This leads to $\delta B \simeq 0.5B_0$, so the wave amplitude would be nearly comparable with the background magnetic field. However, this is likely an overestimate, because when the solar wind arrives at $R \simeq 100$ AU, the plasma has presumably entered the late-time quasi-steady phase during which the energy conversion factor from the kinetic energy of the injected pickup protons to the energy of the magnetic fluctuations is considerably smaller than $\sigma_{pu}$ in the linear temporal growth phase. Finally, if one simply applies equation (5) to near 1 AU where $n_{pu}/n_{sw} \le 10^{-4}$, one gets $(\delta B/B_0)^2 \le 10^{-4}$, so the waves are probably too weak to be observed.

## 5. Summary and Discussion

[37] One-dimensional, self-consistent hybrid simulations are performed to investigate the dynamics of pickup protons in the distant solar wind and the outer heliosheath. In each simulation, freshly ionized protons are continuously injected into a homogeneous, collisionless, relatively cool, background plasma at a constant rate and a velocity perpendicular to the background magnetic field. The simulations first experience a relatively quiescent phase as the pickup protons accumulate and form a ring-velocity distribution, which is unstable to the electromagnetic proton cyclotron instability and eventually leads to enhanced magnetic fluctuations. The magnetic fluctuations then grow exponentially and quickly enter a linear temporal growth phase, which is followed by a late-time quasi-steady phase. In the linear temporal growth phase, our results show that the ratio of the magnetic field energy density growth rate to the injection rate of the pickup proton energy density is essentially independent of both the injection rate and the injection speed of the pickup protons, but decreases with increasing $\beta$ of the background plasma which enhances the proton cyclotron damping of the magnetic fluctuations.

[38] Associated with the growth of the magnetic fluctuations, pickup protons are pitch angle scattered toward an isotropic shell velocity distribution due to wave-particle interactions. The most significant scattering of the pickup protons occurs in the exponential growth phase. The scattering rate of the freshly injected pickup protons during the linear temporal growth phase remains relatively constant and it increases with the pickup proton injection rate. In addition, the simulations reveal that significant pitch angle scattering of the pickup protons occurs after the accumulated pickup proton density exceeds a critical value, the scattering-onset density. The scattering-onset density also increases with the pickup proton injection rate and the scattering onset typically occurs during the exponential growth phase of the magnetic fluctuations.

[39] Scaling relations for the scattering rate and the scattering-onset density versus the pickup proton injection rate are derived from the simulation results. These relations suggest that, although the estimated scattering rate near the heliopause in the outer heliosheath is short enough to broaden the pickup ion velocity distribution on the order of 10 days, it is possible that the scattering onset of the pickup protons does not occur until the interstellar plasma has drifted relatively close to the heliopause so that sufficient pickup protons have accumulated. This is related to the issue of whether the "secondary ENA" mechanism is a possible explanation for the ENA ribbon observed by IBEX [*Heerikhuisen et al.*, 2010], as the pickup protons outside of the scattering-onset distance should remain as a narrow velocity ring and may lead to the narrow ENA ribbon observed by IBEX. Further investigations of this scenario are underway.

[40] In the distant solar wind, our results suggest that the plasma has passed the scattering-onset point given the quick accumulation of the pickup protons. The scattering time of the freshly injected pickup protons is estimated to be about 6 hours upstream of the termination shock at $R \simeq 100$ AU, much shorter than the solar wind transport time. The amplitude of the magnetic fluctuations driven by the pickup protons is estimated to be $\sim 0.5B_0$, which is likely an overestimate as it has not properly considered the effect of the more-slowly growing late-time quasi-steady phase. The results also imply that the waves driven by pickup protons near 1 AU are probably too weak to be observed.

[41] An important limitation of the simulations described here is their one-dimensional character. The condition $\mathbf{k} \times \mathbf{B}_0 = 0$ admits only the fluctuations at the maximum instability growth rate, which through the cyclotron resonance are of prime importance for pitch angle scattering, but does not allow the growth of fluctuations with wave vectors oblique to $\mathbf{B}_0$ which contribute to energy scattering through the proton Landau resonance. A more complete physical picture of the interactions between pickup protons and the enhanced fluctuations which they excite requires at least two-dimensional simulations of these growing modes. Such simulations should be carried out, not only to test the validity of the present results, but also to compare the relative rates of pitch angle scattering versus energy scattering. Furthermore, two-dimensional simulations (particle-in-cell if

not hybrid) will allow us to compute the nonlinear behavior of the proton Bernstein instability [*Liu et al.*, 2011] which may compete with the electromagnetic proton cyclotron instability for generating enhanced magnetic fluctuations from the free energy in pickup proton velocity distributions.

[42] One key element not included in the present study is the effect of background turbulence. It is well established that the solar wind bears a variable but persistent broadband spectrum of magnetic fluctuations with amplitudes monotonically decreasing with increasing observed frequency, and that within a few AU of the Sun this turbulence typically dominates the narrowband enhanced spectra of pickup-ion-driven fluctuations (compare Figures 2 and 3 of *Joyce et al.* [2012]). In contrast, the monotonic increases of the pickup ion injection rates and the pickup proton density with increasing distance from the Sun shown in Figures 2c and 2d suggest that, sufficiently far away from the Sun, enhanced fluctuations driven by the pickup ions could become stronger than the background turbulence, at least at wavelengths resonant with the pickup ions. The recent transport model of solar wind fluctuations by *Oughton et al.* [2011] also supports this picture, predicting that, at distances more than about 10 AU from the Sun, the magnetic energy density of relatively short wavelength Alfvénic fluctuations driven by pickup ions becomes substantially greater than the magnetic energy density of long-wavelength "quasi-2D" turbulence. Still further from the Sun, *Florinski et al.* [2010] estimate that the turbulence from the local interstellar medium in the outer heliosheath is orders of magnitude smaller than the magnetic fluctuations from their hybrid simulations of the electromagnetic (pickup) proton cyclotron instability. Thus, it is likely that broadband turbulence and narrowband enhanced fluctuations driven by pickup ions each contribute to the pitch angle and energy scattering of pickup protons at different solar distances. Further simulations to determine the relative importance of these two sources of such scattering in the solar wind and outer heliosheath should be carried out.

[43] For simplicity, the present simulations neglect the variations of the plasma background, the pickup proton injection rate and the injection velocity. In the solar wind, as a plasma parcel moves away from the Sun, the plasma is subjected to the adiabatic cooling caused by the decrease of the background magnetic field [*Vasyliunas and Siscoe*, 1976]. The pickup proton injection rate and injection velocity (especially the injection angle) also vary. How these factors affect the present results needs future investigations which are beyond the scope of the present study. Nevertheless, the present study provides useful insights on the dynamics of pickup protons in the distant solar wind and the outer heliosheath.

## Appendix A

[44] We denote the $j$th species plasma frequency as $\omega_j \equiv \sqrt{4\pi n_j e_j^2/m_j}$, the $j$th species cyclotron frequency as $\Omega_j \equiv e_j B_o/m_j c$, the $j$th species thermal speed as $v_j \equiv \sqrt{k_B T_{\|j}/m_j}$, $\beta_{\|j} \equiv 8\pi n_j k_B T_{\|j}/B_o^2$. We consider an electron-proton plasma where subscript $e$ denotes electrons and $p$ stands for protons. The cool (few eV) solar wind protons are denoted by subscript *sw*, and the subscript for pickup protons is *pu.* In a proton-electron plasma the Alfvén speed is $v_A \equiv B_o/\sqrt{4\pi n_e m_p}$. We use the symbols $\|$ and $\perp$ to denote directions parallel and perpendicular to $\mathbf{B}_0$, respectively.

[45] **Acknowledgments.** The authors acknowledge useful exchanges with Peter Bochsler. The Los Alamos portion of this work was performed under the auspices of the U.S. Department of Energy (DOE). It was supported by the Solar and Heliospheric Physics SR&T and Heliophysics Guest Investigators Programs of the National Aeronautics and Space Administration (NASA). The research of K.L. was supported by a minigrant from the Institute of Geophysics and Planetary Physics, Los Alamos National Laboratory (LANL), entitled "Pickup Ions and Associated Instabilities Upstream of the Termination Shock". E.M. is grateful for the hospitality of and stimulating collaborations with LANL staff during his work on this project. E.M. gratefully acknowledges the support of the U.S. Department of Energy through LANL's Laboratory Directed Research and Development (LDRD) Program and Institute of Geophysics and Planetary Physics. E.M. was also supported by the IBEX project under contract NNG05EC85C and SR&T grant NNX09AW32G. Computational resources supporting this work were provided by the NASA High-End Computing (HEC) Program through the NASA Advanced Supercomputing (NAS) Division at Ames Research Center.

[46] Philippa Browning thanks the reviewers for their assistance in evaluating this paper.

## References

Axford, W. I. (1972), The interaction of the solar wind with the interstellar medium, in *Solar Wind*, edited by C. P. Sonett, P. J. Coleman, and J. M. Wilcox, pp. 609–660, Sci. and Tech. Inf. Off., NASA, Washington, D. C.

Axford, W. I., A. J. Dessler, and B. Gottlieb (1963), Termination of solar wind and solar magnetic field, *Astrophys. J.*, *137*, 1268–1278.

Bzowski, M., E. Möbius, G. Gloeckler, S. Tarnopolski, and V. Izmodenov (2008), Density of neutral interstellar hydrogen at the termination shock from Ulysses pickup ion observations, *Astron. Astrophys.*, *491*(1), 7–19, doi:10.1051/0004-6361:20078810.

Bzowski, M., et al. (2012), Neutral interstellar helium parameters based on IBEX-Lo observations and test particle calculations, *Astrophys. J. Suppl. Ser.*, *198*, 12, doi:10.1088/0067-0049/198/2/12.

Cowee, M. M., C. T. Russell, and R. J. Strangeway (2008), One-dimensional hybrid simulations of planetary ion pickup: Effects of variable plasma and pickup conditions, *J. Geophys. Res.*, *113*, A08220, doi:10.1029/2008JA013066.

Fahr, H. J. (1968), Neutral corpuscular energy flux by charge-transfer collisions in the vicinity of the Sun, *Astrophys. Space Sci.*, *2*, 496–503, doi:10.1007/BF02175924.

Florinski, V., G. P. Zank, J. Heerikhuisen, Q. Hu, and I. Khazanov (2010), Stability of a pickup ion ring-beam population in the outer heliosheath: Implications for the IBEX ribbon, *Astrophys. J.*, *719*, 1097–1103.

Funsten, H. O., et al. (2009), Structures and spectral variations of the outer heliosphere in IBEX energetic neutral atom maps, *Science*, *326*, 964–966, doi:10.1126/science.1180927.

Fuselier, S. A., et al. (2009), Width and variation of the ENA flux ribbon observed by the Interstellar Boundary Explorer, *Science*, *326*, 962–964, doi:10.1126/science.1180981.

Gamayunov, K., M. Zhang, and H. Rassoul (2010), Pitch angle scattering in the outer heliosheath and formation of the Interstellar Boundary EXplorer ribbon, *Astrophys. J.*, *725*, 2251–2261.

Gary, S. P. (1991), Electromagnetic ion/ion instabilities and their consequences in space plasmas: A review, *Space Sci. Rev.*, *56*, 373–415, doi:10.1007/BF00196632.

Gary, S. P. (1993), *Theory of Space Plasma Microinstabilities*, Cambridge Univ. Press, New York.

Gary, S. P., and C. D. Madland (1988), Electromagnetic ion instabilities in a cometary environment, *J. Geophys. Res.*, *93*(A1), 235–241, doi:10.1029/JA093iA01p00235.

Gary, S. P., S. Hinata, C. D. Madland, and D. Winske (1986), The development of shell-like distributions from newborn cometary ions, *Geophys. Res. Lett.*, *13*(13), 1364–1367, doi:10.1029/GL013i013p01364.

Gary, S. P., C. D. Madland, N. Omidi, and D. Winske (1988), Computer simulations of two-pickup-ion instabilities in a cometary environment, *J. Geophys. Res.*, *93*(A9), 9584–9596, doi:10.1029/JA093iA09p09584.

Gary, S. P., K. Akimoto, and D. Winske (1989), Computer simulations of cometary-ion/ion instabilities and wave growth, *J. Geophys. Res.*, *94*(A4), 3513–3525, doi:10.1029/JA094iA04p03513.

Gary, S. P., R. H. Miller, and D. Winske (1991), Pitch-angle scattering of cometary ions: Computer simulations, *Geophys. Res. Lett.*, *18*(6), 1067–1070, doi:10.1029/91GL01331.

Heerikhuisen, J., et al. (2010), Pick-up ions in the outer heliosheath: A possible mechanism for the Interstellar Boundary Explorer ribbon, *Astrophys. J.*, *708*, L126, doi:10.1088/2041-8205/708/2/L126.

Isenberg, P. A., C. W. Smith, W. H. Matthaeus, and J. D. Richardson (2010), Turbulent heating of the distant solar wind by interstellar pickup protons in a decelerating flow, *Astrophys. J.*, *719*(1), 716–721, doi:10.1088/0004-637X/719/1/716.

Joyce, C. J., C. W. Smith, P. A. Isenberg, N. Murphy, and N. A. Schwadron (2010), Excitation of low-frequency waves in the solar wind by newborn interstellar pickup ions $H^+$ and $He^+$ as seen by Voyager at 4.5 AU, *Astrophys. J.*, *724*(2), 1256–1261, doi:10.1088/0004-637X/724/2/1256.

Joyce, C. J., C. W. Smith, P. A. Isenberg, S. P. Gary, N. Murphy, P. C. Gray, and L. F. Burlaga (2012), Observations of Bernstein waves excited by newborn interstellar pickup ions in the solar wind, *Astrophys. J.*, *745*(2), 112, doi:10.1088/0004-637X/745/2/112.

Lindsay, B. G., and R. F. Stebbings (2005), Charge transfer cross sections for energetic neutral atom data analysis, *J. Geophys. Res.*, *110*, A12213, doi:10.1029/2005JA011298.

Liu, K., S. P. Gary, and D. Winske (2011), Excitation of magnetosonic waves in the terrestrial magnetosphere: Particle-in-cell simulations, *J. Geophys. Res.*, *116*, A07212, doi:10.1029/2010JA016372.

McComas, D. J., et al. (2004), The Interstellar Boundary Explorer (IBEX), in *Physics of the Outer Heliosphere: Third International IGPP Conference*, edited by V. Florinski, N. V. Pogorelov, and G. P. Zank, *AIP Conf. Proc.*, *719*, 162–181.

McComas, D. J., et al. (2009), Global observations of the interstellar interaction from the Interstellar Boundary Explorer (IBEX), *Science*, *326*, 959–962, doi:10.1126/science.1180906.

McComas, D. J., et al. (2010), Evolving outer heliosphere: Large-scale stability and time variations observed by the interstellar boundary explorer, *J. Geophys. Res.*, *115*, A09113, doi:10.1029/2010JA015569.

McComas, D. J., et al. (2012), The heliosphere's interstellar interaction: No bow shock, *Science*, *336*, 1291–1293, doi:10.1126/science.1221054.

McKean, M. E., N. Omidi, and D. Krauss-Varban (1995), Wave and ion evolution downstream of quasi-perpendicular bow shocks, *J. Geophys. Res.*, *100*(A3), 3427–3437, doi:10.1029/94JA02529.

Möbius, E., et al. (2012), Interstellar gas flow parameters derived from IBEX-Lo observations in 2009 and 2010: Analytical analysis, *Astrophys. J. Suppl. Ser.*, *198*(2), 11, doi:10.1088/0067-0049/198/2/11.

Murphy, N., E. J. Smith, B. T. Tsurutani, A. Balogh, and D. J. Southwood (1995), Further studies of waves accompanying the solar wind pick-up of interstellar hydrogen, *Space Sci. Rev.*, *72*, 447–452, doi:10.1007/BF00768819.

Omidi, N., and D. Winske (1986), Simulation of the solar wind interaction with the outer regions of the Coma, *Geophys. Res. Lett.*, *13*(4), 397–400, doi:10.1029/GL013i004p00397.

Oughton, S., W. H. Matthaeus, C. W. Smith, B. Breech, and P. A. Isenberg (2011), Transport of solar wind fluctuations: A two-component model, *J. Geophys. Res.*, *116*, A08105, doi:10.1029/2010JA016365.

Richardson, J. D. (1997), The heliosphere-interstellar medium interaction: One shock or two?, *Geophys. Res. Lett.*, *24*(22), 2889–2892, doi:10.1029/97GL02973.

Richardson, J. D. (2008), Plasma temperature distributions in the heliosheath, *Geophys. Res. Lett.*, *35*, L23104, doi:10.1029/2008GL036168.

Richardson, J. D., J. C. Kasper, C. Wang, J. W. Belcher, and A. J. Lazarus (2008a), Cool heliosheath plasma and deceleration of the upstream solar wind at the termination shock, *Nature*, *454*, 63–66, doi:10.1038/nature07024.

Richardson, J. D., Y. Liu, C. Wang, and D. J. McComas (2008b), Determining the LIC H density from the solar wind slowdown, *Astron. Astrophys.*, *491*(1), 1–5, doi:10.1051/0004-6361:20078565.

Schwadron, N. A., et al. (2009), Comparison of interstellar boundary explorer observations with 3D global heliospheric models, *Science*, *326*, 966–968, doi:10.1126/science.1180986.

Stone, E. C. (2001), News from the edge of interstellar space, *Science*, *293*, 55–56, doi:10.1126/science.1060090.

Vasyliunas, V. M., and G. L. Siscoe (1976), On the flux and the energy spectrum of interstellar ions in the solar system, *J. Geophys. Res.*, *81*(7), 1247–1252, doi:10.1029/JA081i007p01247.

Winske, D., and M. M. Leroy (1984), Diffuse ions produced by electromagnetic ion beam instabilities, *J. Geophys. Res.*, *89*(A5), 2673–2688, doi:10.1029/JA089iA05p02673.

Winske, D., and N. Omidi (1993), Hybrid codes: Methods and applications, in *Computer Space Plasma Physics: Simulation Techniques and Software*, edited by H. Matsumoto and Y. Omura, pp. 103–160, Terra Sci., Tokyo.

Winske, D., and K. B. Quest (1988), Magnetic field and density fluctuations at perpendicular supercritical collisionless shocks, *J. Geophys. Res.*, *93*(A9), 9681–9693 doi:10.1029/JA093iA09p09681.

Wu, C. S., D. Winske, and J. D. Gaffey Jr. (1986), Rapid pickup of cometary ions due to strong magnetic turbulence, *Geophys. Res. Lett.*, *13*(8), 865–868, doi:10.1029/GL013i008p00865.

Wu, P., D. Winske, S. P. Gary, N. A. Schwadron, and H. O. Funsten (2009), Energy dissipation and ion heating at the heliospheric termination shock, *J. Geophys. Res.*, *114*, A08103, doi:10.1029/2009JA014240.

Zank, G. P. (1999), Interaction of the solar wind with the local interstellar medium: A theoretical perspective, *Space Sci. Rev.*, *89*, 413–688, doi:10.1023/A:1005155601277.

Zank, G. P., H. L. Pauls, I. H. Cairns, and G. M. Webb (1996a), Interstellar pickup ions and quasi-perpendicular shocks: Implications for the termination shock and interplanetary shocks, *J. Geophys. Res.*, *101*(A1), 457–477, doi:10.1029/95JA02860.

Zank, G. P., H. L. Pauls, L. L. Williams, and D. T. Hall (1996b), Interaction of the solar wind with the local interstellar medium: A multifluid approach, *J. Geophys. Res.*, *101*(A10), 21,639–21,655, doi:10.1029/96JA02127.